

IMAGES IN THE ROCKET ULTRAVIOLET: THE INITIAL HELIUM ABUNDANCE AND DISTANCE MODULUS OF THE GLOBULAR CLUSTER M5 FROM PHOTOMETRY OF HORIZONTAL-BRANCH STARS

RALPH C. BOHLIN

Space Telescope Science Institute

ROBERT H. CORNETT AND JESSE K. HILL

Systems and Applied Sciences Corporation

AND

ANDREW M. SMITH AND THEODORE P. STECHER

Laboratory for Astronomy and Solar Physics, Goddard Space Flight Center

Received 1984 September 21; accepted 1984 December 3

ABSTRACT

The globular cluster M5 (NGC 5904) was observed in the ultraviolet with a rocket-borne telescope to obtain images at effective wavelengths for hot stars near 1540 Å and 2360 Å with bandpasses of 340 Å and 990 Å. Of the 144 stars whose positions were determined to 1'6, 84 have been observed from the ground and are to the blue of the RR Lyrae gap. We have used our 2360 Å magnitude along with the *V* magnitude to determine effective temperatures and bolometric corrections for 50 stars using model atmospheres. Applying the horizontal-branch models of Sweigart and Gross for $Z = 0.001$, we determine best fit model parameters $Y = 0.21$, distance modulus 14.39, and helium core mass $0.492 M_{\odot}$. The luminosity-effective temperature diagram has the slope predicted by standard horizontal-branch models, neglecting rotation. From the hottest horizontal-branch star observed, we estimate a maximum mass loss prior to the horizontal-branch phase of $\sim 0.3 M_{\odot}$. A second UV bright star was discovered, with $T_e \approx 40,000$ K and $L \approx 400 L_{\odot}$, assuming membership in M5.

Subject headings: clusters: globular — stars: abundances — stars: atmospheres — stars: evolution — stars: horizontal branch — ultraviolet: general

I. INTRODUCTION

Globular clusters provide a natural laboratory for the study of post-main sequence evolution of low-mass ($< 1 M_{\odot}$) metal-poor stars. As such, they are critical for developing an understanding of advanced stages of stellar evolution and of the chemical evolution of the Galaxy. They can also provide constraints for models of element formation in the early universe. Photometric results from a rocket observation of the cluster M5 in bandpasses centered at 1540 and 2360 Å are reported here.

Observations in the rocket ultraviolet are useful for isolating stars representing the hotter stages ($T_e \gtrsim 10^4$ K) of evolution. The brightest globular cluster stars in the ultraviolet are expected to be blue horizontal-branch stars and post-asymptotic giant branch stars, which may also be planetary nebula nuclei. The cooler background main-sequence stars, red horizontal-branch stars, and all but the brightest red giants are effectively suppressed. Combining our photometric results with recent ground-based photometry of Buonanno, Corsi, and Fusi Pecci (1981, hereafter BCF) and using stellar evolutionary models of Sweigart and Gross (1976, 1978), we derive estimates for the initial helium abundance Y and dereddened distance modulus ($m - M$)₀. Ground-based photometry has also been done by Simoda and Tanikawa (1970) and by Arp (1962).

Our previous investigation of the post-asymptotic branch star near the center of M5 is described by Bohlin *et al.* (1983*b*). Here, we investigate the fainter horizontal-branch stars. In § II we describe the rocket payload and data reduction procedure. Source identification, astrometry, and photometry are discussed in § III, while fits to evolutionary models and determi-

nation of helium abundance, distance modulus, and limits on mass loss are discussed in § IV. The discovery of a second UV-bright star is also described in § IV.

II. OBSERVATIONS AND DATA REDUCTION

a) Payload and Flight Data

The payload, the prototype for our Astro Spacelab instrument (Stecher *et al.* 1983), consisted of a 38 cm *f*/9.0 Ritchey-Chrétien telescope with two electrostatically focused ITT microchannel plate image intensifiers coupled to Kodak IIa-O film, as described by Bohlin *et al.* (1983*a, b*). The bandpass of the short-wavelength camera was defined by the response of a CsI photocathode with a calcium fluoride filter to eliminate geocoronal Ly α emission, while the long-wavelength bandpass was determined by the response of a CsTe cathode plus a quartz filter, with a short-wavelength cutoff around 1600 Å. The parameters describing the payload optics plus detector system are given in Table 1.

Eight flight exposures of M5 were obtained, with exposure times 1 s, 5 s, and 25 s, for the CsI camera, and 0.2 s, 1 s, and 5 s for the CsTe camera, with the intermediate exposure time repeated in each case. Spatial resolution was limited by rocket pointing stability to about 8" (FWHM) on the CsTe and shorter CsI exposures, but was degraded to 8" \times 20" on the 25 s CsI exposure due to drift in the pointing.

b) Preflight Bandpass Calibration

The bandpasses of the two cameras were determined from preflight calibration data by the method described by Bohlin *et al.*

TABLE 1
INSTRUMENTAL PARAMETERS

Parameter	Value
Optics:	
Focal ratio	f/9.0
Primary diameter	38.0 cm
Number of reflecting surfaces	4 (Al + MgF ₂)
Plate scale	1'00 ± 0'001 mm ⁻¹
Detectors:	
Type	ITT Microchannel plate
Windows	CaF ₂ (short wavelength) quartz (long wavelength)
Cathodes	
	CsI (short wavelength) CsTe (long wavelength)
Diameter	40 mm
Output	Phosphor/fiber optics
Data	70 mm Kodak IIA-O
System resolution	80 μm (5")
Flight:	
Date	0615 UT 1982 Apr 17
Place	White Sands Missile Range
Rocket	Black Brant 27.059
Point system	STRAP V
Limit cycle	3"

al. (1982). Figure 1 shows the relative response as a function of wavelength for the two cameras for a constant energy spectrum, normalized to unity at the peak. Maximum sensitivity occurs at a wavelength of 1540 Å for the CsI camera and 2360 Å for the CsTe camera. The bandwidths, defined as the integral of the response function over wavelength, are 340 Å and 990 Å for the CsI and CsTe cameras, respectively.

c) Reduction of Flight Data

The steps followed in digitizing and reducing the image data to relative intensity were similar to those followed in the reduction of the Orion Nebula and M101 image data obtained

on previous flights of a similar instrument, as described by Bohlin *et al.* (1982) and Hill, Bohlin, and Stecher (1984). All flight frames and laboratory calibration images were digitized on a PDS 1010a microdensitometer, using a 20 μm (1"2) square aperture, resulting in 2048 × 2048 pixel images. We corrected for drift of the PDS response with time by additively adjusting all densities in each scan line by a smooth function of scan line to give a uniform fog level for regions on the film outside the field of view. Subset images with 20' × 20' fields centered on M5 were boxaveraged to 512 × 512 arrays of 40 μm pixels after conversion of the measured photographic density (*D*) to linear relative intensity (*H*).

The *H* and *D* curve consisted of a 1024 element lookup table for the 10 bit PDS density digitization and was determined for densities less than about 1.5 from a series of flat-field laboratory exposures taken with geometrically increasing exposure times. For higher densities, the *H* and *D* curve was determined by requiring that the flight frames give consistent photometric results for the brighter sources, including the UV-bright star in M5 and the nuclear source in M83 reported earlier (Bohlin *et al.* 1983*a, b*). Vignetting and nonuniformities in the sensitivity of the photocathodes were removed by dividing by smoothed laboratory flat-field exposures. The accuracy of the conversion to relative intensity and flat fielding is estimated from the reproducibility of the brightest individual sources and aperture photometry of the cluster as a whole to be about 10% over the density range 0.3–3.0, or a dynamic range of about 200 in exposure.

We determined the absolute calibration using the method described by Bohlin *et al.* (1982), in which UV spectra of standard sources which appear on the flight images are integrated over the rocket payload bandpass to determine an average flux at the effective wavelength. In this case the standards used were the UV-bright star and the nuclear source in M83, as observed by us with the *IUE* SWP and LWR cameras in low dispersion.

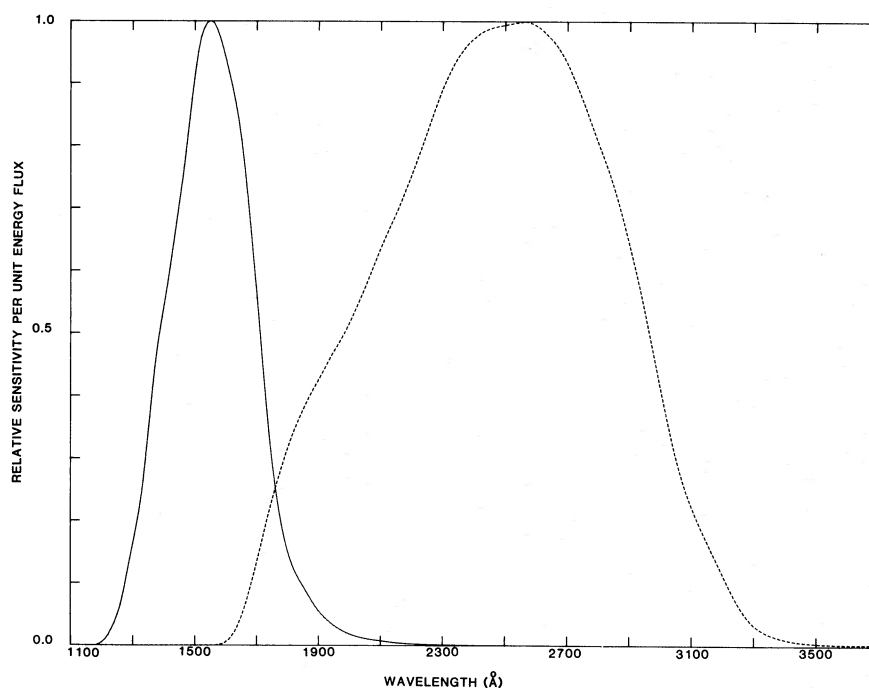


FIG. 1.—Relative spectral sensitivity of the CsI camera (solid line) and CsTe camera (dashed line), each normalized to unity at the peak

Photometry of these two sources on the flight exposures then determined the conversion factors between relative intensities and flux in absolute units. The accuracy of the absolute *IUE* calibration is about 10%.

III. DETERMINATION OF FLUXES AND POSITIONS OF STARS

a) Star Selection, Position Measurement, and Identification

Candidate sources whose distances from the cluster center are greater than $2'$ and less than $10'$ and whose peak densities are greater than about 0.5 on the CsTe 5 s exposure were selected for further study. A total of 144 sources were selected.

Positions of 317 stars in M5 have been determined by Cudworth (1979), while Hogg (1973) has given positions for 103 variables. We identified 26 candidates from our list with stars whose positions were determined by Cudworth or Hogg and computed a plate solution from them. Positions were then computed relative to the cluster center for all 144 stars to an estimated accuracy of $1''.6$. Using the finding charts of BCF we identified 86 sources with stars for which they determined *B* and *V* magnitudes photographically, one of which is an unresolved blend of two stars separately measured by BCF. Our list includes 84 of the 93 blue horizontal-branch stars of BCF (including both possible contributors to the blend), 14 of the 55 RR Lyrae stars of Hogg which are in the area we searched, and three of the 30 red horizontal-branch stars of BCF. Of the nine blue horizontal-branch stars of BCF not identified with stars on our list, four are inside our $2'$ boundary, and five are below our detection limit. We have measured fluxes for seven stars which are within the area searched by BCF but which are not identifiable with any of their measured stars. These will be further discussed in § IV.

Figure 2 (Plate 6) is the 5 s CsTe exposure with the stars selected for further study labeled in order of increasing right ascension.

b) Photometry

Fluxes were determined on the 5 s CsTe exposure for each source free of discernible contamination from neighboring stars by integrating over a 7×7 pixel ($16''.8$) aperture. For stars less than $4'$ from the cluster center, a sky correction varying with radial distance was applied. For 40 stars with near neigh-

bors, photometry was performed using smaller apertures, including either 9, 21, or 40 pixels, depending on the degree of contamination. The total flux obtained was then scaled according to values obtained from a point spread function determined from an average over a set of unblended sources. For 12 sources the crowding was so severe that reliable photometry was not possible.

From the consistency of the photometry on the 5 s and the two 1 s exposures, the relative fluxes are accurate to $\sim 20\%$ on the 5 s exposure. Using the absolute calibration determined from our *IUE* observations of the UV-bright star near the cluster center (Bohlin *et al.* 1983b), and a nominal quantum efficiency of 5% for the system, including mirror reflectivities, filter transmissions, and photocathode efficiency, we would expect ~ 30 detected photons on the 5 s CsTe exposure for a star with a typical flux of 2.0×10^{-15} ergs cm^{-2} s^{-1} \AA^{-1} . We conclude that the count statistics of the detected photons is the major contributor to the observational error. For computing best fit models in § IV, we adopt a detective quantum efficiency (DQE) of 3.3% derived directly from the observed *S/N*.

Fluxes were determined on the 25 s CsI exposure by integrating over an aperture modified to take account of the trailing of the image. A uniform sky level determined from the mean surface brightness over several apparently source-free areas was subtracted. Because of the trailing, the errors in the CsI camera photometry are somewhat greater, especially for the fainter stars measured.

Figure 3 is a color-color diagram for the blue horizontal-branch stars plotting $\log (F_{1540}/F_{2360})$ versus $\log F_{2360} + 0.4V$. The plotted curves show the colors predicted by the model atmospheres of Kurucz (1979) for heavy element abundances 0.1 of solar (*solid line*) and 0.01 solar (*dashed line*), for surface gravities appropriate for horizontal-branch stars. In principle such a diagram can be used to determine *Z*. Unfortunately, as the model atmospheres show, the $\log (F_{1540}/F_{2340})$ color discriminates most sensitively between different abundances for the cooler stars, for which the CsI photometry is most uncertain. For the model fitting described in § IV, we used the 0.1 solar metal abundance models, in agreement with the value tabulated by Harris and Racine (1979).

Table 2 gives the measured positions and fluxes in our band-passes for the 144 sources satisfying the search criteria. The

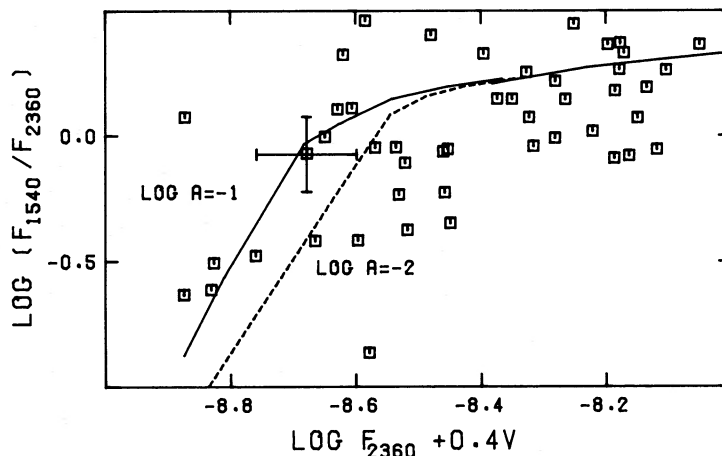


FIG. 3.— $\log (F_{1540}/F_{2360})$ vs. $\log F_{2360} + 0.4V$ for 50 observed horizontal-branch stars (boxes) and model atmospheres for metal abundances 0.1 solar (*solid line*) and 0.01 solar (*dashed line*). For $T_e > 10,000$ K, solar abundance models are plotted as a solid line.

PLATE 6

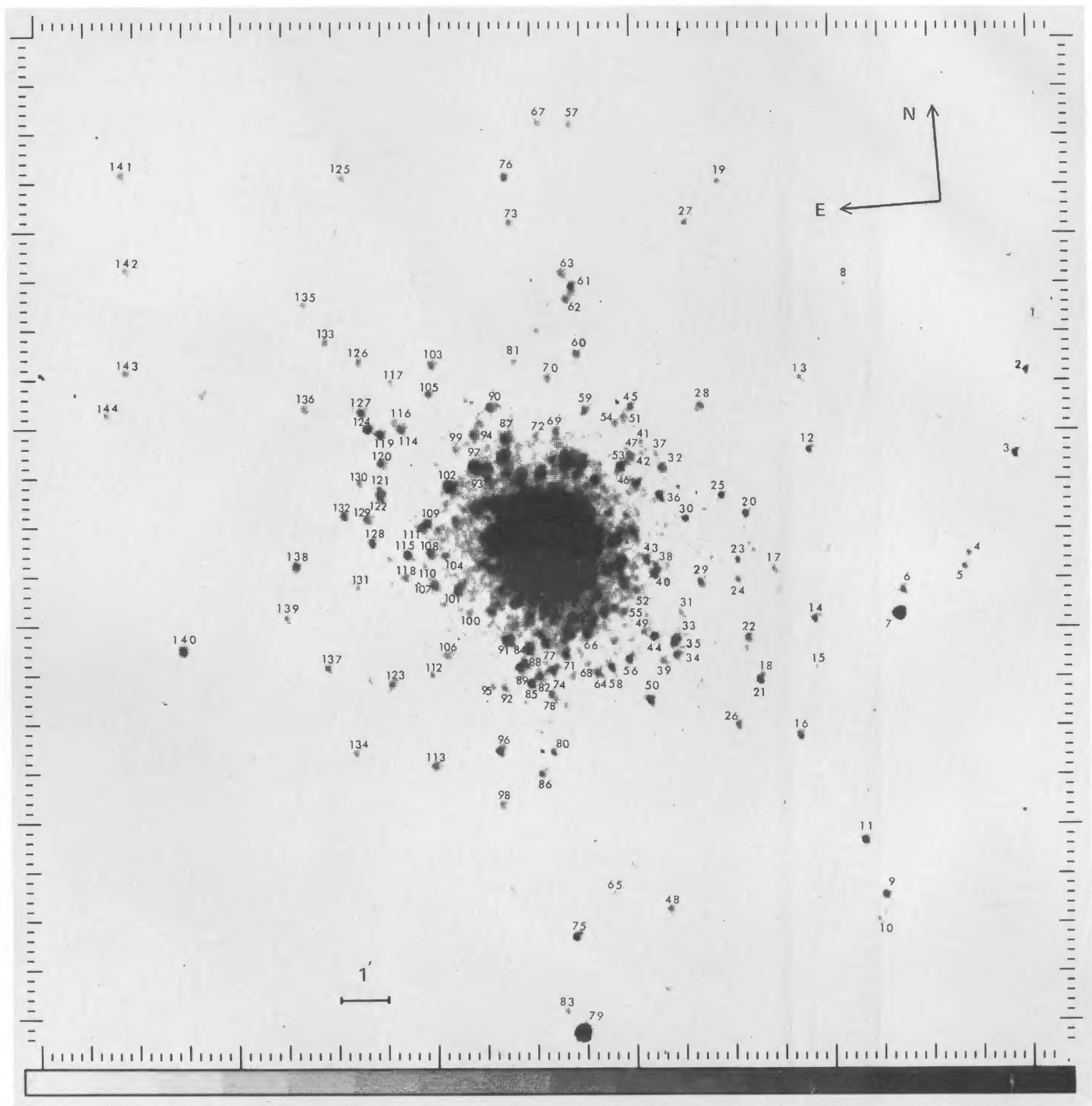


FIG. 2.—The 5 s CsTe exposure of M5 with star numbers from Table 2

BOHLIN *et al.* (see page 689)

TABLE 2
OBSERVED STELLAR PARAMETERS

Number (1)	Identifi- cation (2)	Member Code (3)	X (arcsec) (4)	Y (arcsec) (5)	$F_{2360} \times 10^{15}$ (ergs cm ⁻² s ⁻¹ Å ⁻¹) (6)	CsTe Code (7)	$F_{1540} \times 10^{15}$ (ergs cm ⁻² s ⁻¹ Å ⁻¹) (8)	CsI Code (9)
1.....	-626.2	231.4	0.80	1	0.50	1
2.....	-606.4	170.1	1.9	1	0.80	1
3.....	-583.2	67.9	2.6	1	<0.27	1
4.....	Z185	M	-515.0	-47.2	1.1	3	0.69	1
5.....	-508.7	-63.9	1.7	2	<0.27	1
6.....	-431.0	-86.7	2.5	1	0.4	1
7.....	Z206	X	-424.0	-115.1	12	1	0.93	1
8.....	-394.7	291.5	0.96	1	<0.27	1
9.....	-375.4	-458.3	2.7	1	3.6	1
10.....	Z216	M	-365.7	-486.5	1.4	1	1.2	1
11.....	-356.7	-389.1	3.0	1	6.5	1
12.....	-331.8	93.2	2.2	1	1.2	1
13.....	-329.4	183.0	1.6	1	<0.27	1
14.....	-321.8	-112.1	2.6	1	<0.27	1
15.....	Z235	X	-319.0	-172.2	1.1	1	0.58	1
16.....	-289.5	-257.5	2.5	1	4.7	1
17.....	-276.0	-47.7	1.6	1	3.7	1
18.....	-250.4	-176.6	1.4	4	3.4	1
19.....	Z270	X	-250.0	429.3	1.5	1	0.37	1
20.....	II-15	M	-247.7	22.6	2.2	1	1.0	1
21.....	III-86	M	-247.3	-183.5	2.4	4	6.7	2
22.....	III-22	M	-237.2	-129.5	2.4	1	2.1	1
23.....	III-2	X	-233.1	-34.4	1.7	1	1.3	1
24.....	III-17	M	-231.0	-58.3	1.7	1	1.5	1
25.....	II-100	...	-220.3	46.7	2.1	1	1.9	1
26.....	III-91	M	-215.6	-236.7	2.3	1	1.3	1
27.....	-207.0	382.0	1.7	1	2.2	1
28.....	II-46	...	-205.4	159.3	2.4	1	1.9	1
29.....	III-117	M	-184.8	-57.0	2.1	1	4.4	1
30.....	II-14	M	-174.3	21.3	1.4	1	0.48	1
31.....	V65	...	-157.2	-93.6	0.82	1	<0.27	1
32.....	II-41	...	-150.4	86.2	2.4	3	<0.27	1
33.....	III-37	M	-150.0	-121.9	...	99	<0.27	1
34.....	III-43	M	-148.0	-143.7	1.9	3	<0.27	1
35.....	III-38	...	-147.0	-126.5	...	99	<0.27	1
36.....	II-22	...	-145.3	52.8	2.3	1	0.98	1
37.....	V14	M	-144.7	103.7	0.54	4	<0.27	1
38.....	V79	...	-133.3	-33.8	0.58	4	1.2	1
39.....	III-46	M	-130.5	-149.4	1.6	1	2.0	1
40.....	III-10	...	-129.9	-43.1	...	99	3.3	1
41.....	-128.9	119.5	0.54	3	<0.27	1
42.....	II-52	M	-127.8	105.0	...	99	<0.27	1
43.....	III-8	...	-121.7	-25.5	...	99	1.2	1
44.....	V42	M	-120.9	-119.7	3.0	3	0.42	1
45.....	II-82	X	-120.5	163.9	1.7	2	<0.27	1
46.....	II-30	...	-117.1	67.2	2.3	1	<0.27	1
47.....	II-53	...	-113.0	103.8	1.9	4	2.6	1
48.....	Z346	M	-112.4	-453.3	1.9	1	<0.27	1
49.....	III-34	M	-111.8	-111.8	1.2	3	2.7	1
50.....	III-55	...	-111.8	-196.5	2.9	1	3.0	1
51.....	II-81	X	-109.7	152.5	1.9	4	<0.27	1
52.....	III-112	...	-106.5	-60.8	1.4	1	0.42	1
53.....	II-37	...	-99.7	90.4	...	99	4.7	1
54.....	II-78	M	-99.5	146.1	1.4	2	<0.27	1
55.....	III-33	...	-90.0	-83.6	1.2	1	0.29	1
56.....	III-58	...	-89.6	-143.5	2.3	2	4.2	1
57.....	Z466	X	-76.9	513.8	1.6	1	1.5	1
58.....	III-65	...	-67.0	-151.4	1.1	4	5.8	1
59.....	II-72	...	-64.3	163.6	1.5	1	2.0	1
60.....	II-114	...	-60.5	234.0	2.2	1	2.5	1
61.....	II-119	...	-60.3	316.5	3.3	3	3.6	1
62.....	II-127	M	-54.2	300.0	2.4	2	1.4	1
63.....	II-118	...	-49.7	334.3	2.1	2	2.1	1
64.....	III-68	...	-49.5	-157.4	2.2	2	3.0	1
65.....	Z448	M	-46.2	-428.5	1.2	1	<0.27	1
66.....	III-142	...	-41.7	-108.6	3.2	1	6.9	1
67.....	Z553	X	-38.3	519.4	1.8	1	<0.27	1
68.....	III-69	M	-38.3	-146.7	...	99	<0.27	1
69.....	II-62	...	-25.7	140.1	1.0	3	<0.27	1
70.....	II-87	...	-22.0	208.1	1.4	1	3.5	1
71.....	III-71	...	-12.8	-132.9	1.9	1	4.1	1
72.....	V51	...	-1.6	137.2	0.65	1	<0.27	1

TABLE 2—Continued

Number (1)	Identifi- cation (2)	Member Code (3)	X (arcsec) (4)	Y (arcsec) (5)	$F_{2360} \times 10^{15}$ (ergs cm ⁻² s ⁻¹ Å ⁻¹) (6)	CsTe Code (7)	$F_{1540} \times 10^{15}$ (ergs cm ⁻² s ⁻¹ Å ⁻¹) (8)	CsI Code (9)
73.....	Z629	M	5.7	399.5	1.9	1	1.4	1
74.....	III-72	...	5.9	-150.5	2.7	3	6.5	1
75.....	6.9	-479.9	2.8	1	3.6	1
76.....	8.3	455.4	2.7	1	3.9	1
77.....	10.2	116.5	2.4	3	4.9	1
78.....	IV-94	...	11.0	-179.0	1.5	1	0.34	1
79.....	11.6	-595.9	23.0	1	80.0	1
80.....	III-83	M	14.3	-249.2	1.7	1	1.6	1
81.....	V41	M	17.3	230.7	1.2	1	0.48	1
82.....	IV-120	M	21.0	-156.5	...	99	7.0	2
83.....	Z601	X	26.3	-568.0	1.2	1	<0.27	1
84.....	IV-1+IV-2	...	30.1	-122.1	3.3	3	6.7	1
85.....	IV-17	...	31.3	-163.0	2.9	2	6.9	1
86.....	IV-20	M	31.3	-276.8	2.1	1	0.29	1
87.....	I-6	...	37.7	138.0	2.9	1	2.3	1
88.....	IV-5	M	38.7	-136.0	...	99	3.7	1
89.....	44.2	-142.9	2.3	3	6.3	1
90.....	I-161	M	53.7	178.1	2.0	1	2.8	1
91.....	IV-8	...	55.6	-108.1	3.6	1	10.0	1
92.....	IV-31	...	65.8	-167.5	1.7	3	<0.27	1
93.....	I-134	...	72.3	104.4	...	99	14.0	2
94.....	I-51	...	73.7	143.4	2.2	1	2.6	1
95.....	V55	M	77.6	-164.1	1.3	3	<0.27	1
96.....	IV-21	...	79.4	-243.8	3.1	1	4.6	1
97.....	I-11	...	79.6	104.9	2.7	3	11.0	2
98.....	IV-96	...	80.0	-309.1	2.0	1	<0.27	1
99.....	I-48	M	97.1	128.3	1.2	1	<0.27	1
100.....	98.9	-72.7	0.47	1	0.32	1
101.....	111.1	-42.6	2.6	1	5.2	1
102.....	I-16	...	113.2	83.5	3.9	1	3.3	1
103.....	I-63	M	117.3	234.3	2.3	1	2.0	1
104.....	V87	...	122.3	-0.4	1.3	3	<0.27	1
105.....	I-117	...	125.2	198.7	1.9	1	4.4	1
106.....	V28	...	129.9	-121.0	1.5	1	<0.27	1
107.....	IV-50	...	137.4	-35.4	2.2	1	3.4	1
108.....	IV-57	...	139.2	3.6	2.3	3	4.2	1
109.....	140.9	42.4	2.2	3	8.3	1
110.....	147.8	-12.6	...	99	<0.27	1
111.....	I-29	...	148.4	38.3	1.7	3	7.2	2
112.....	V31	M	151.5	-143.7	1.1	1	<0.27	1
113.....	IV-125	...	158.6	-256.8	2.6	1	4.2	1
114.....	I-69	...	160.2	158.0	2.1	3	3.9	2
115.....	IV-58	...	168.4	3.6	2.4	1	2.4	1
116.....	I-70	...	169.2	168.5	1.3	4	2.4	1
117.....	I-66	...	170.0	219.5	1.5	1	4.4	1
118.....	IV-60	M	173.0	-22.6	1.4	1	<0.27	1
119.....	I-84	...	187.5	155.6	3.3	3	5.3	1
120.....	I-44	M	190.5	121.8	2.5	1	0.95	1
121.....	V9	...	193.4	85.3	...	99	0.93	1
122.....	I-37	...	194.0	80.6	3.5	3	3.6	1
123.....	V32	M	201.1	-151.7	2.4	1	<0.27	1
124.....	V74	...	204.0	164.2	2.7	3	0.95	1
125.....	205.0	471.9	1.5	1	4.4	1
126.....	I-103	...	206.8	246.7	1.9	1	3.7	2
127.....	I-72	...	209.3	186.3	2.8	1	2.6	1
128.....	I-34	...	210.7	24.0	2.3	1	3.3	1
129.....	V63	M	213.1	53.4	2.5	1	2.1	1
130.....	I-41	...	219.6	97.2	1.6	1	1.6	1
131.....	IV-68	M	232.1	-27.5	1.1	1	1.3	1
132.....	I-108	...	241.8	58.2	2.7	1	6.2	1
133.....	246.1	274.1	1.8	1	2.5	1
134.....	IV-107	...	251.8	-232.4	1.9	1	1.7	1
135.....	266.3	321.9	1.7	1	2.4	1
136.....	I-152	...	277.3	192.0	2.2	1	3.1	2
137.....	IV-105	...	279.5	-125.9	2.1	1	3.8	1
138.....	IV-115	...	305.4	2.7	3.0	1	5.4	1
139.....	IV-117	...	322.7	-59.1	1.7	1	0.66	1
140.....	454.6	-89.6	3.8	1	6.5	1
141.....	473.7	498.8	2.0	1	3.0	1
142.....	Z974	M	479.0	380.8	1.6	1	2.8	1
143.....	492.0	255.5	1.9	1	6.3	1
144.....	520.5	206.7	1.8	1	3.3	1

number in column (1) corresponds to the label in Figure 2. Column (2) gives identification numbers, which are in the notation of Arp for stars measured by BCF, or prefixed by a V for Hogg variables, or by a Z for stars first measured by Zhukov (1971). Column (3) is a membership code based on the proper motion results of Cudworth (1979): M, if the probability of membership is greater than 50%; X, if the probability of membership is less than 50%; and blank if no membership results are available. Columns (4) and (5) give the right ascension and declination in arc seconds relative to the cluster center in the 1950.0 coordinate system of Hogg. Column (6) gives the CsTe bandpass flux in units of 10^{-15} ergs cm^{-2} s^{-1} \AA^{-1} at the effective wavelength (typically 2300 \AA for lightly reddened B stars). Column (7) is a reliability code for the CsTe photometry based upon the degree of blending of the stellar image with neighboring stars, ranging from 1 (no detectable contamination) to 4 (serious contamination—flux reported based on scaling from only 9 pixels). For even more severe contamination, no flux is reported in column (6) and a reliability code of 99 is entered in column (7); 12 such cases exist. Column (8) gives the CsI bandpass flux in units of 10^{-15} ergs cm^{-2} s^{-1} \AA^{-1} at the effective wavelength (typically 1530 \AA for a B star). Column (9) is a reliability code for the CsI photometry: 1 for stars not seriously affected by image crowding and 2 for stars for which crowding may be significant. The fluxes reported in such cases should probably be regarded as upper limits, since they were computed in the same way as for the apparently uncontaminated stars. Upper limit fluxes of 0.27×10^{-15} are reported for some of the cooler stars which show no significant CsI flux.

IV. DISCUSSION

a) The Helium Abundance and Distance of M5

Previous workers have estimated the helium abundance and distance modulus of M5 using a variety of methods. Buzzoni *et al.* (1983) obtained $Y = 0.20 \pm 0.03$ using the ratio of the number of horizontal-branch stars to the number of red giants and their relative lifetimes from models. BCF obtained $Y = 0.22$ from the color of the blue edge of the RR Lyrae instability strip, applying results of pulsation theory. Harris (1974) determined a distance modulus $(m - M)_0 = 14.42$ [assuming $E(B - V) = 0.03$] from the V magnitudes of the RR Lyrae stars, while Carney (1980) obtained $(m - M)_0 = 14.24$ from matching the main sequence to evolutionary models, implicitly assuming $Y = 0.19 \pm 0.04$, as previously determined for local subdwarfs (Carney 1979). From the magnitudes of the RR Lyrae stars compared to those in M3, Sandage (1982) obtained $(m - M)_0 = 14.18$.

The shape and normalization of the M5 horizontal branch locus in the observational $\log F_{2360} - V$ plane can also be used to estimate the initial helium abundance Y and distance modulus. The energy generation of the hotter and less massive horizontal-branch stars is dominated by the helium-burning core; that of the cooler and more massive stars, by the hydrogen-burning shell. These two processes have opposite Y dependencies, so that with increasing Y , the luminosity of the cooler stars increases relative to the hotter ones. As a result, the shape of the horizontal branch changes.

A spread in mass is assumed to account for the spread in temperature along the horizontal branch in the $L - T_e$ plane. The temperature spread along the horizontal branch could also be due in part to a distribution of core masses associated

with a spread in rotational velocities (Rood 1973; Demarque, Mengel, and Sweigart 1972); however, Peterson (1983) has found no evidence for significant rotation ($> 15 \text{ km s}^{-1}$) for a sample of seven HB stars in M5 from high-dispersion optical spectroscopy.

b) Fitting Y and $(m - M)_0$ Using Evolutionary Models

Our procedure for determining best fit values of helium abundance and distance modulus is closely related to the method of Flannery and Johnson (1982) for fitting observations of two independent quantities x and y to a model characterized by a curve in the x - y plane. In this case, we have a sample of horizontal-branch stars with measured V (from BCF) and F_{2360} . Because of evolution of the stars away from the zero-age horizontal branch, we must fit the observations to a two-dimensional region of the V - F_{2360} plane, rather than a curve. For given helium abundance and distance modulus, the two independent random variables mass and age from the zero-age horizontal branch determine a position in the V - F_{2360} plane.

Sweigart and Gross (1976, 1978) have constructed evolutionary model sequences for both red giant and horizontal-branch stars, neglecting rotation and mass loss. Horizontal-branch models are tabulated for various combinations of four independent variables, namely core mass M_c , envelope helium abundance Y_{HB} , heavy element abundance Z , and total mass. We adopt $Z = 10^{-3}$, consistent with the value given in the review by Harris and Racine (1979). Y_{HB} and M_c were determined as functions of the initial helium abundance Y from the red giant model sequences, as the core mass and envelope helium abundance at the time of helium flash. Y_{HB} is slightly greater than Y because of convective dredge-up on the red giant branch. Loci in the $L - T_e$ plane were determined for $Y = 0.10$ – 0.30 for stars on the zero-age horizontal branch, midway through horizontal-branch evolution, and near the end of horizontal-branch evolution. Interpolation between tabulated models was performed where necessary. The horizontal-branch loci were then transformed to the observational $V - F_{2360}$ plane using the LTE model atmospheres of Kurucz (1979) with metal abundances 0.1 solar and surface gravities determined from the evolutionary models. Non-LTE effects are not expected to be important for blue horizontal-branch stars (Rossi 1979). The models were reddened to a color excess $E(B - V)$ of 0.03 (Burstein and McDonald 1975). Distance moduli in the range 14.00–15.00 were considered.

For each distance modulus and helium abundance considered, we computed, for every observed star i , a probability $p(v^i, F_{2360}^i)$ from the equation

$$p(v^i, F_{2360}^i) = \frac{1}{2\pi} \iint \exp \left\{ -\frac{[F_{2360}^i - F_{2360}(M, t)]^2}{2\sigma_{uv}^2} - \frac{[V^i - V(M, t)]^2}{2\sigma_v^2} \right\} f(M) dM dt, \quad (1)$$

where the integrals are over time since the zero-age horizontal branch and total mass. Equation (1) is a straightforward generalization of equation (7) of Flannery and Johnson (1982) for a two-parameter model and observations with differing variances. In evaluating the integral, the weighting function $f(M)$ is assumed to be constant. The variances σ_v^2 and σ_{uv}^2 are from the quoted uncertainties of BCF and the count statistics of detected UV photons, assuming a DQE of 3.3% for the

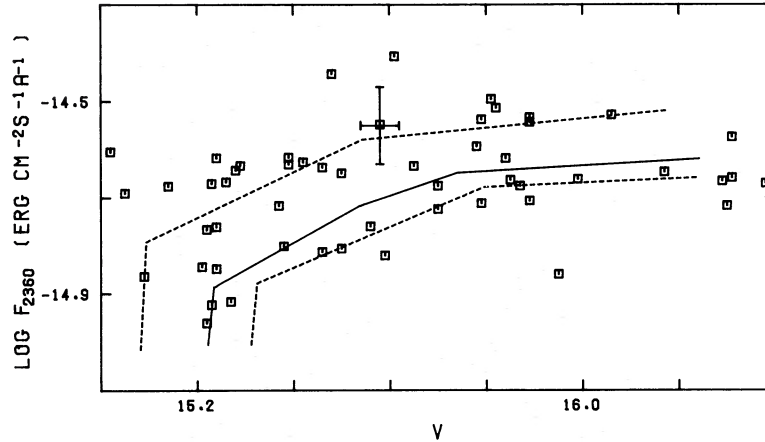


FIG. 4.— $\text{Log } F_{2360}$ vs. V for 50 horizontal-branch stars (boxes) together with the curves for zero age (lower dashed line), mean age (solid line), and maximum age (upper dashed line) horizontal-branch sequences for the best fit model parameters $Y = 0.21$ and $(m - M)_0 = 14.39$.

CsTe camera derived directly from the repeatability of fluxes measured on different exposures. The integral over M was evaluated using the near-point estimator method described by Flannery and Johnson. The integral over t was evaluated as a weighted sum over the three evolutionary states, with zero age and maximum age weighted by 0.50.

For each helium abundance and distance modulus we then computed the statistic $S = -2 \sum_i \log p(V^i, F_{2360}^i)$, where the sum is over the 50 observed stars whose CsTe camera photometry was judged most reliable (reliability codes 1 or 2), excluding one star whose cluster membership probability was estimated to be 40% by Cudworth (1979). (We do not anticipate any significant contamination of our sample by nonmembers, since it is unlikely that any foreground white dwarfs or distant halo main-sequence stars would have UV and optical magnitudes undistinguishable from those of blue horizontal-branch stars at the distance of M5.) We determined best fit model parameters from the position of the centroid of $\exp(-S/2)$ in the $(m - M)_0$ - Y plane, obtaining $Y = 0.21$ and $(m - M)_0 = 14.39$. The horizontal-branch core mass is then $0.492 M_\odot$. Figure 4 shows the observed points and the best fit model in the observational coordinates V and $\log F_{2360}$. Figure 5 shows the data and best fit models in the theoretical L - T_e diagram. The minimum value of S is 1.1 per degree of freedom, suggesting that all of the variance between the data

and the best fit model can be accounted for by the known sources of photometric error.

As Lampton, Margon, and Bowyer (1976) have emphasized, the best fitting model parameters are of little interest without an estimate of the volume of parameter space required to contain the true values of the parameters with a given probability. We assume that S is distributed as χ^2 with 48 degrees of freedom and use the fact that $\Delta S = S - S_{\min}$ is distributed as χ^2 with 2 degrees of freedom. We then determine the regions in the $(m - M)_0$ - Y plane which include the true values of the parameters with 70% probability and 90% probability, corresponding roughly to 1.0σ and 1.65σ uncertainty levels for Gaussian statistics. Using the boundary of the 70% probability region to determine error bars, we find acceptable models for $Y = 0.19$ – 0.24 and $(m - M)_0 = 14.29$ – 14.51 .

The best fit distance modulus for each value of Y is strongly correlated with Y , ranging from 14.27 for $Y = 0.18$ to 14.66 for $Y = 0.28$. Figure 6 shows the 70% and 90% probability ΔS contours in the $(m - M)_0$ - Y plane, while Figure 7 plots ΔS versus Y for the best fitting distance modulus corresponding to each value of Y . The acceptable distance modulus interval results in a corresponding interval for the absolute magnitude M_v of the RR Lyrae stars of 0.52 – 0.74 , which is consistent with the observed range of 0.6 ± 0.3 , using the observed $V = 15.11$ for the RR Lyrae stars in M5 (Harris 1974).

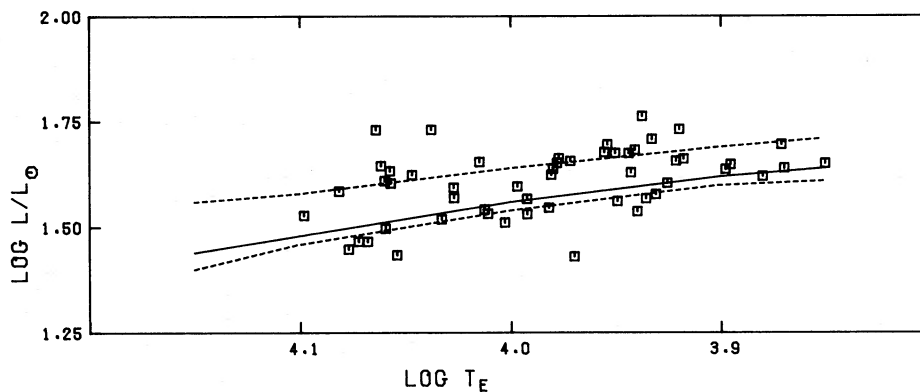


FIG. 5.—Luminosity vs. effective temperature for 50 horizontal-branch stars (boxes), together with the curves for zero age (lower dashed line), mean (solid line), and maximum age (upper dashed line) horizontal-branch sequences for the best fit model parameters $Y = 0.21$ and $(m - M)_0 = 14.39$.

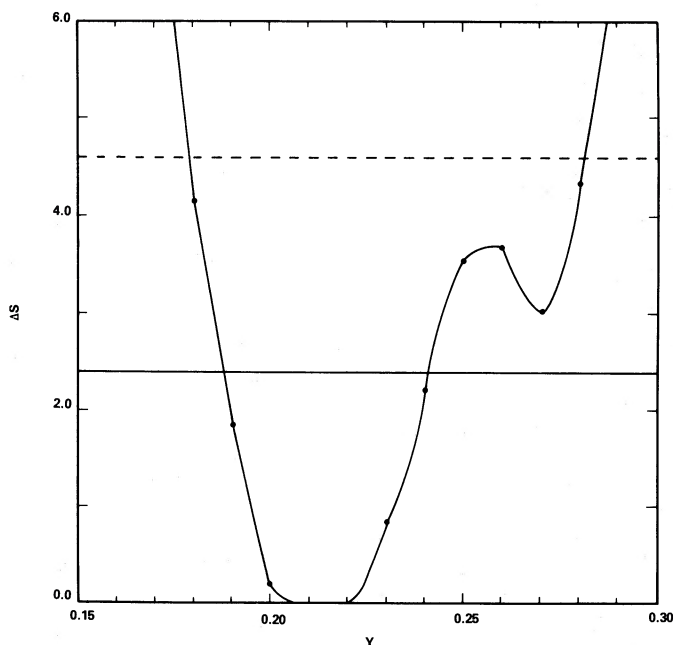


FIG. 6.—Contours enclosing the true values of Y and $(m - M)_0$ with 70% probability (solid line) and 90% probability (dashed line). The contours are interpolated between the points corresponding to the models actually computed.

Although our best fit initial helium abundance Y is in satisfactory agreement with results obtained by BCF, the horizontal-branch locus in the L - T_e plane which we infer from the CsTe camera flux and their V magnitudes is not in good agreement with the horizontal-branch locus they derive from B and V magnitudes. Their horizontal branch locus rises to higher luminosities at the higher temperatures, which, as they point out, is not in agreement with horizontal-branch model calculations. The source of the disagreement appears to be in the colors of the bluest stars, for which an error in $B - V$ can introduce a large error in the inferred bolometric correction,

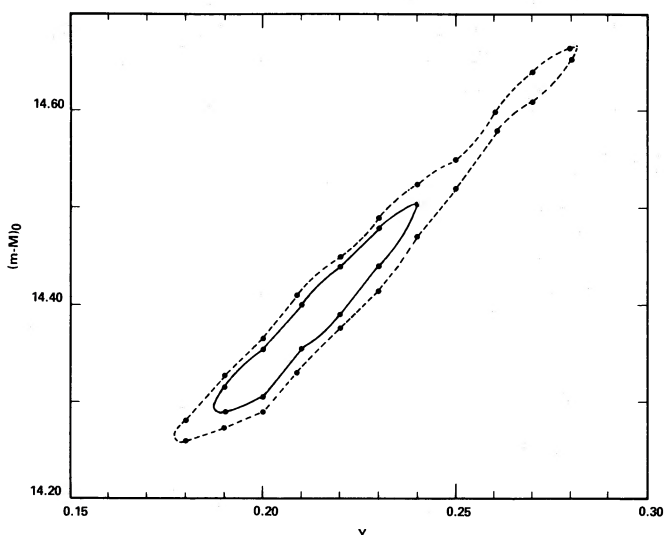


FIG. 7.— ΔS vs. Y for the best fitting distance modulus at each Y together with the S levels bounding the 70% probability region (solid line) and 90% probability region (dashed line).

and, therefore, the luminosity. Thus, if statistical error in $B - V$ is a significant contribution to the population of the blue end of their observed horizontal branch, the inferred horizontal-branch locus in the L - T_e plane would be expected to have the slope reported by BCF. The calibration difficulties which they experienced for the bluest stars may also play a role. Since our CsTe bandpass fluxes determine T_e with greater leverage, our results would not be so sensitive to small errors in observed V or $\log F_{2360}$.

The value of Y deduced from observations of globular clusters should provide a reliable upper limit to the amount of helium produced by nucleosynthesis in the early universe. The amount of helium synthesis predicted by the standard models depends upon three parameters, namely the half-life of the neutron, the number of species of light neutrinos, and the baryon-to-photon ratio (Olive *et al.* 1981). Although our results confine Y with 70% probability to the interval 0.19–0.24, Yang *et al.* (1984) find that a more precise determination is necessary, if the three parameters of cosmology and particle physics are to be closely constrained. A more precise determination of Y could be made using the methods of this paper, if the CsTe photometry were accurate to 0.10 mag, a result which is well within capabilities of the Ultraviolet Imaging Telescope (Stecher *et al.* 1983). Observations of the redder horizontal-branch stars will also be possible. More precise photometry is useful for more stringent tests of the existing horizontal-branch and red giant evolutionary models, since the width of the observed horizontal branch contributed by evolutionary effects would then dominate the observational uncertainty.

c) Minimum Observed Horizontal-Branch Mass and Inferences on Mass Loss

The hottest of the 50 stars used in the model fits is number 132 in Table 2, identified with I-108 from BCF, with $T_e = 13,500$ K and $L = 40 L_\odot$, for $(m - M)_0 = 14.39$. We infer a mass of 0.50–0.55 M_\odot from the models of Sweigart and Gross. As the bluest star in our sample of horizontal-branch stars, it would, therefore, be the least massive. A main-sequence turn-off mass of $\sim 0.8 M_\odot$ then implies mass loss of up to about 0.3 M_\odot between the main sequence and the horizontal branch. Since the red giant models of Sweigart and Gross do not include mass loss, strict consistency with the assumptions of the models requires that the mass loss take place during the transition from the red giant branch to the zero-age horizontal branch.

It is important for determining the maximum amount of mass loss to be sure that one has found the hottest blue horizontal-branch star in the region searched. Within the region searched by BCF, we find two stars satisfying our search criteria which have CsTe bandpass reliability codes less than 3, but which are not identified with any of the BCF stars. If these are horizontal-branch stars hotter than I-108, we would expect the CsTe flux to be comparable to or greater than that of I-108. In fact, star 17 has a CsTe flux about 0.6 that of I-108. The other star, number 100, is only 0.2 as bright in the CsTe bandpass and is, therefore, unlikely to be a horizontal-branch star. The possibility that star 17 is a horizontal-branch star can not be ruled out; however, we can conclude that there is no significant population of horizontal branch stars in M5 bluer than I-108. Ultraviolet observations are important for establishing this fact, since, unlike ground-based observations in the V bandpass, the hotter horizontal-branch stars appear as bright as or brighter than the cooler horizontal-branch stars.

d) Individual UV-Bright Stars

The best fit distance modulus can be used to derive a revised effective temperature estimate for the UV-bright post-AGB star discussed by Bohlin *et al.* (1983b). We assume that the star is traversing the H-R diagram at a constant luminosity approximately equal to the luminosity at the red giant tip, or $\sim 2000 L_{\odot}$. For a distance modulus of 14.39, we then derive an effective temperature of $\sim 38,000$ K, from the *IUE* spectral data of Bohlin *et al.* (1983b). The mass-luminosity relation for thermally pulsing AGB stars (Paczynski 1970) gives a mass of $0.53 M_{\odot}$, consistent with the HB core mass of $0.492 M_{\odot}$ which the red giant models of Sweigart and Gross (1978) predict for an initial helium abundance of 0.21, allowing for an increase in core mass during the HB and AGB evolution (Sweigart and Gross 1976).

Another star of particular interest is number 79, which is the brightest star in both the UV bandpasses within the area which we searched, with UV fluxes about 0.2 of the UV-bright star

near the cluster center. Star 79 does not correspond with any of the stars measured by Cudworth, so its membership in the cluster is not firmly established. Since it is outside the area investigated by BCF, no visual photometry is available. From the ratio of fluxes in the two UV bandpasses, we estimate $T_e \approx 40,000$ K. If star 79 is at the distance of M5, the luminosity is $\sim 400 L_{\odot}$. It is certainly in an advanced stage of evolution, whether or not it is a cluster member, since on the main sequence a star of effective temperature 40,000 K would have luminosity $\sim 2 \times 10^4 L_{\odot}$ and, therefore, be at a distance 200 kpc to give the UV fluxes we observe. Possibly star 79 is also a post-AGB star which is now in the pre-white dwarf cooling phase.

We thank the Sounding Rocket staff at Goddard Space Flight Center for their essential assistance in obtaining the data for this paper. We are also grateful to Dr. A. Sweigart and Dr. M. Schwarzschild for valuable discussions of stellar evolution in globular clusters.

REFERENCES

- Arp, H. 1962, *Ap. J.*, **135**, 311.
 Bohlin, R. C., Cornett, R. H., Hill, J. K., Smith, A. M., and Stecher, T. P. 1983a, *Ap. J. (Letters)*, **274**, L53.
 Bohlin, R. C., Cornett, R. H., Hill, J. K., Smith, A. M., Stecher, T. P., and Sweigart, A. V. 1983b, *Ap. J. (Letters)*, **267**, L89.
 Bohlin, R. C., Hill, J. K., Stecher, T. P., and Witt, A. N. 1982, *Ap. J.*, **255**, 87.
 Buonanno, R., Corsi, C. E., and Fusi Pecci, F. 1981, *M.N.R.A.S.*, **196**, 435 (BCF).
 Burstein, D., and McDonald, L. H. 1975, *A.J.*, **80**, 17.
 Buzzoni, A., Fusi Pecci, F., Buonanno, R., and Corsi, C. E. 1983, *Astr. Ap.*, **128**, 94.
 Carney, B. W. 1979, *Ap. J.*, **233**, 877.
 ———. 1980, *Ap. J. Suppl.*, **42**, 481.
 Cudworth, K. M. 1979, *A.J.*, **84**, 1866.
 Demarque, P., Mengel, J. G., and Sweigart, A. V. 1972, *Ap. J. (Letters)*, **173**, L27.
 Flannery, B. P., and Johnson, B. C. 1982, *Ap. J.*, **263**, 166.
 Harris, W. E. 1974, *A.J.*, **81**, 1095.
 Harris, W. E., and Racine, R. 1979, *Ann. Rev. Astr. Ap.*, **17**, 241.
 Hill, J. K., Bohlin, R. C., and Stecher, T. P. 1984, *Ap. J.*, **277**, 542.
 Hogg, H. S. 1973, *Pub. David Dunlap Obs.*, **3**, No. 6.
 Kurucz, R. L. 1979, *Ap. J. Suppl.*, **40**, 1.
 Lampton, M. L., Margon, B., and Bowyer, S. 1976, *Ap. J.*, **208**, 177.
 Olive, K. A., Schramm, D. N., Steigman, G., Turner, M. S., and Yang, J. 1981, *Ap. J.*, **246**, 557.
 Paczynski, B. 1970, *Acta Astr.*, **19**, 1.
 Peterson, R. C. 1983, *Ap. J.*, **275**, 737.
 Rood, R. T. 1973, *Ap. J.*, **184**, 815.
 Rossi, L. 1979, *Astr. Ap.*, **74**, 195.
 Sandage, A. 1982, *Ap. J.*, **252**, 553.
 Simoda, M., and Tanikawa, K. 1970, *Pub. Astr. Soc. Japan*, **22**, 143.
 Stecher, T. P., Bohlin, R. C., Butcher, H. R., O'Connell, R. W., Roberts, M. S., Smith, A. M., and Parise, R. A. 1983, *Bull. AAS*, **14**, 882.
 Sweigart, A. V., and Gross, P. G. 1976, *Ap. J. Suppl.*, **32**, 367.
 ———. 1978, *Ap. J. Suppl.*, **36**, 405.
 Yang, J., Turner, M. S., Steigman, G., Schramm, D. N., and Olive, K. O. 1984, *Ap. J.*, **281**, 493.
 Zhukov, L. V. 1971, *Trudy Pulkova Obs.*, Ser. 2, **78**, 160.

RALPH C. BOHLIN: Space Telescope Science Institute, Homewood Campus, Baltimore, MD 21218

ROBERT H. CORNETT and JESSE K. HILL: Systems and Applied Sciences Corporation, 5809 Annapolis Road, Hyattsville, MD 20784

ANDREW M. SMITH and THEODORE P. STECHER: Code 680, Laboratory for Astronomy and Solar Physics, Goddard Space Flight Center, Greenbelt, MD 20771